The interaction mechanism between bovine serum albumin and single-walled carbon nanotubes depending on their diameter and concentration in solid bionanocomposites

Gerasimenko, Alexander Yu.

Alexander Yu. Gerasimenko, "The interaction mechanism between bovine serum albumin and single-walled carbon nanotubes depending on their diameter and concentration in solid bionanocomposites," Proc. SPIE 11363, Tissue Optics and Photonics, 113631P (2 April 2020); doi: 10.1117/12.2554935

SPIE.

Event: SPIE Photonics Europe, 2020, Online Only, France

The interaction mechanism between bovine serum albumin and single-walled carbon nanotubes depending on their diameter and concentration in solid bionanocomposites

Alexander Yu. Gerasimenko[a,b]
[a] National Research University of Electronic Technology MIET, Bld. 1, Shokin Square, Zelenograd, Moscow, Russia, 124498; [b]I.M. Sechenov First Moscow StateMedical University, 2-4 Bolshaya Pirogovskaya st., Moscow, Russia, 119991

ABSTRACT

A method for formation of bionanocomposites that can be used as coatings for implantable devices interacting with blood is proposed. Such bionanocomposites are composed of albumin blood protein and single-walled carbon nanotubes (SWCNT). They are formed by evaporation of water-albumin dispersion of nanotubes by diode laser with precise temperature control. In this work influence of various types of SWCNT graphene structure defects on formation of frame structure from them and albumin was determined using Raman and FTIR spectroscopy methods. It was found that shape of graphene sheet affects the intensity of the D and D' bands in its Raman spectrum. Strongest increase in the intensity of D band compared to G band is observed in case of partial or complete absence of hydrogen atoms at the boundary of graphene sheet, which leads to practical disappearance of G and D' lines in Raman spectrum. Molecular modeling showed that for structural defects of graphene sheet edge there is a steric hindrance, which occurs when vibrations of neighboring hydrogen atoms moving towards each other. Possibility of SWCNT functionalization by oxygen atoms of negative amino acid residues aspartic (Asp) and glutamic (Glu), which are located on the outer surface of BSA, is demonstrated. Formation of covalent bonds between BSA and SWCNTs is confirmed by FTIR and Raman spectra. Spectra were recorded for small diameter nanotubes (1.7 nm) with various concentrations (0.01, 0.1, and 1 g/mol). An increase in concentration of nanotubes leads to saturation of functionalization of SWCNTs with oxygen atoms of amino acid residues Asp and Glu. Covalent interaction of BSA with SWCNTs disrupts secondary and tertiary albumin structure. This is confirmed by significant decrease in absorption bands intensity in high-frequency region. Formation of covalent bond between BSA and SWCNTs in composite leads to an increase in band intensity in ~1330 cm^{-1} region on Raman spectrum compared to the spectrum of initial nanotubes. This confirms presence of significant defects in SWCNTs caused by covalent addition of oxygen to graphene surface of nanotubes. It was found that increase in diameter of nanotubes (4 nm) and their concentration in composite practically does not affect vibrational spectra, which confirms the hydrophobic interaction of BSA and SWCNTs. Thus, two types of interactions in solid composites based on BSA with SWCNT – hydrophobic and with formation of covalent bonds – depend on the diameter of nanotubes used. This criterion makes it possible to widely use frame composites to control the state of blood cells aggregation.

Keywords: laser radiation, Raman spectra, bovine serum albumin, carbon nanotubes, bionanocomposites, FTIR

1. INTRODUCTION

Recently, methods for synthesis of new nanomaterials have been actively developed to create scaffolds for tissue engineering, biosensors and drugs for theranostics[1-6]. Functional nanomaterials that provide control over the state of aggregation of blood cells are especially important[7-10]. In medicine and biology, carbon nanotubes (CNTs) have proven themselves well. CNTs have sizes close to the sizes of main natural cell matrix components, their mechanical properties are similar to properties of protein structures[11-13]. Mechanical, electrical, optical, and thermal properties of nanotubes are well studied and can be changed as a result of their modifications by external sources[14]. Adding nanotubes to biopolymer matrices allows to obtain biocomposites. As such biopolymers, proteins or single amino acids are mainly used[15]. In many works, it was found that interaction of CNTs with molecules of main biopolymers (albumin, collagen, DNA, ribonuclease etc.) occurs due to non-covalent interaction. For example, conformational analysis of biomolecules showed a stable van der Waals interaction for the DNA-CNT complex. Albumin protein is used as a dispersing agent for single-walled carbon nanotubes (SWCNTs) functionalized with carboxyl groups[16,17]. Decrease in fluorescent signal from

Tissue Optics and Photonics, edited by Valery V. Tuchin, Walter C. P. M. Blondel, Zeev Zalevsky, Proc. of SPIE Vol. 11363, 113631P · © 2020 SPIE
CCC code: 0277-786X/20/$21 · doi: 10.1117/12.2554935

albumin upon the addition of nanotubes indicates a hydrophobic interaction of amino acid residues of protein with nanotubes. A well-known application of albumin and nanotube-based composites was its use for detection of colon bacillus[18]. Nanotubes were injected with blood plasma, after which albumin adsorption to nanotubes was observed to create composites. Authors of [19] linked albumin to the surface of nanotubes for vector drug delivery. Binding efficiency was demonstrated using Raman spectroscopy. Raman spectra, fluorescence and circular dichroism spectra demonstrated hydrophobic interactions (hydrogen bonds, Van der Waals forces, electrostatic forces) and π-stacking as the main mechanisms of interaction of SWCNT with BSA[20].

An urgent task of modern technology is creation of bionanocomposites with frame base of nanotubes in protein matrix for various applications[21–24]. Fundamental possibility of obtaining composites by laser method was shown in[25-26]. Nanotube framework was formed as a result of evaporation of water-albumin dispersion of carbon nanotubes. Formation of C-C bonds occurs in the region of defects of neighboring carbon nanotubes in framework under the influence of laser heating[14]. As it is known, synthesis of nanotubes in graphene plane, from which SWCNTs are formed, contains a fairly large number of defects. Raman spectroscopy is used to determine the imperfection of carbon nanomaterials. Especially this type of spectroscopy is relevant for SWCNTs. They are also called graphene nanotubes. Raman spectra of graphene have several characteristic bands D, G, D' and 2D[27-29]. D band indicates defects caused by imperfection of lattice and presence of impurities[30]. To control defectiveness, it is necessary to determine the ratio of G and D bands intensities[28]. For samples with low number of defects, D line intensity is several orders of magnitude lower than G line intensity[31]. If the intensities of these lines are proportional, this indicates a rather large number of defects in graphene structure of SWCNT. Nature of the origin of D band is explained by Raman resonance scattering at the optical phonon near K-point of the Brillouin zone[32]. Since the 2D line, by its nature, corresponds to double resonance Raman scattering, it can also be observed in defect-free graphene. Calculation and comparison of D and 2D lines intensities showed comparable values in presence of defects in graphene, and intensities of G and D' lines have a very low values. Of great interest is relation of the D, D', and 2D bands to each other and to the type of structural defects. In [33], the influence of three types of graphene defects on the intensities ratio of D and D' lines was considered. In particular, a change in hybridization from sp2 to sp3 due to functionalization, introduction of atoms into lattice structure, changes in shape of graphene edges and formation of vacancies inside the lattice. It was found that intensity coefficient of D and D' peaks is maximum (13) for sp3 defects, decreases for vacancy defects (7), and reaches a minimum for defects at graphite boundary (3.5). In this regard, it becomes necessary to determine which particular defect can affect the appearance or magnitude of 2D band intensity. Since this will help to clarify the features of frame structure formation mechanism due to interaction of SWCNTs and biopolymer – bovine serum albumin (BSA).

Frame structure based on SWCNTs and BSA promotes self-organization of various biological tissues cells. It is supported by non-covalent bonds in hydrophobic interaction of biological tissues. Similar organization of biological macromolecules in nature is found in plasma cell membranes (phospholipids). It has been previously demonstrated that graphene surface of SWCNT can interact with BSA through hydrophobic forces. However, when creating solid framework bionanocomposites, covalent bonds between BSA and SWCNTs can be formed, which can be carried out under the influence of laser radiation.

The aim of this work was to determine the mechanism of interaction of single-walled carbon nanotubes with BSA using vibrational spectroscopy of bionanocomposites. For this, Raman spectra and absorption spectra in the IR region of composites with different concentrations and diameters of SWCNTs were studied. Raman spectra of SWCNT graphene plane with various types of defects were also theoretically calculated and analyzed.

2. METHODOLOGY

2.1 Theoretical study

Theoretical studies were carried out by the method of quantum chemical modeling and density functional theory (DFT) in the Gaussian program. For modeling, fragment of graphene sheet with the shape of parallelogram, which has the smallest defect (Figure 1), was chosen. And also similar fragment of graphene with hydrogen atoms around the perimeter. The main attention is paid to vacancy violation of hexagonal structure, which is located on the edge of graphene sheet. The evolution of atomic and molecular structures in time and space with different number of hydrogen atoms in the environment was studied using molecular dynamics method. Implementation of this method requires determination of interatomic interaction potential, for example, Lennard-Jones potential.

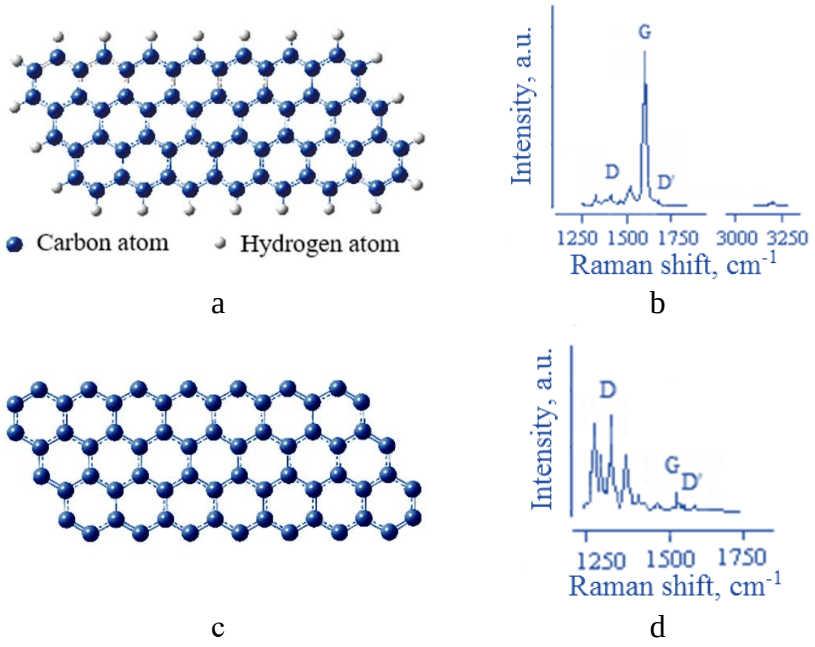

Figure 1. Molecular model of graphene sheet in the form of parallelogram with and without hydrogen atoms (a) (b). Their Raman spectra in the presence of hydrogen (c) and without it (d).

In order to stabilize the zwitterions in solid phase of bionanocomposite, Polarized Continuum Model (SCRF-PCM) was used. In this model, volume into which studied molecule is placed represents a set of overlapping van der Waals spheres constructed along isoplastic lines.

2.2 Experimental study

For manufacturing of bionanocomposites, an aqueous-protein dispersion of SWCNTs and BSA was initially created. Albumin is widely used as a laser solder, which is applied to laser-welded biological tissues[34–36]. BSA is well studied at atomic-structural level: albumin molecule has two modifications (isomers), which are an ellipsoid of revolution and an irregular triangular prism[37]. As filler of albumin matrix, two types of SWCNTs were used. Nanotubes of the first type (SWCNT 1) were synthesized by electric arc method on a Ni/Y catalyst, purified in a mixture of HNO_3/H_2SO_4, followed by washing to a neutral reaction. Average nanotube diameter was ~1.4–1.8 nm, length was 0.3–0.8 μm, and the specific surface area was ~ 400 m^2/g. Purity of SWCNTs was 98%. Figure 1a shows the image of SWCNTs transmission electron microscopy. Nanotubes of the second type (SWCNT 2) were obtained by gas-phase synthesis and purified by a similar method as the first type SWCNT 1. Average diameter was 3.2–4 nm, their length was about 5 microns, and specific surface area was 420 m^2/g. Degree of purity of SWCNT 2 was 91%. Thus, main difference between types of nanotubes was their geometric dimensions (Figure 2).

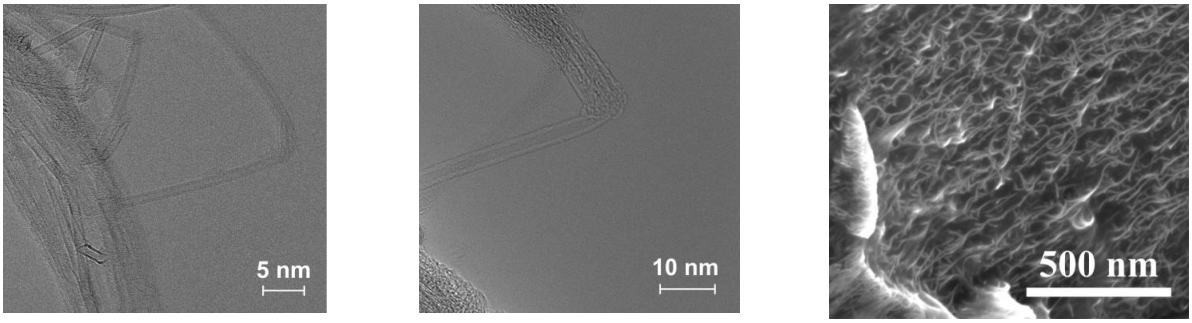

a b c

Figure 2. Transmission electron microscopy images of small SWCNT 1 (a) and large SWCNT 2 (b) and scanning electron microscopy image of cleaved bionanocomposite based on BSA and SWCNT 1 with concentration 1 g/L (c)

Nanotubes were dispersed in water using an ultrasonic homogenizer to prepare a water-protein dispersion. Next, BSA (concentration ~25 wt.%) in the form of a powder was added to aqueous dispersion of nanotubes and was first mixed with magnetic stirrer and then in ultrasonic bath. Method of producing bionanocomposites was as follows. First, water-albumin dispersion was deposited on silicon substrate, then it was irradiated with laser radiation (Figure 3). Diode laser (810 nm) was used for irradiation. Laser radiation power was about 3 W. In order to prevent strong heating and protein denaturation during the preparation of composites, temperature of irradiated dispersion was controlled and maintained in range of 60-80°C. For this, IR temperature sensor and a feedback system connecting laser and sensor were used. The denaturation temperature of used BSA was determined by differential scanning calorimetry and was about 85.7°C. Laser radiation was applied until water component of dispersion was evaporated. As a result of irradiation, bionanocomposites was formed in solid phase state. Concentration of nanotubes was ~0.001, 0.01, and 0.1 wt.%, or 0.01, 0.1, and 1 g/L. Studies of physicochemical properties of aqueous dispersions and composites are described in detail in[21-26].

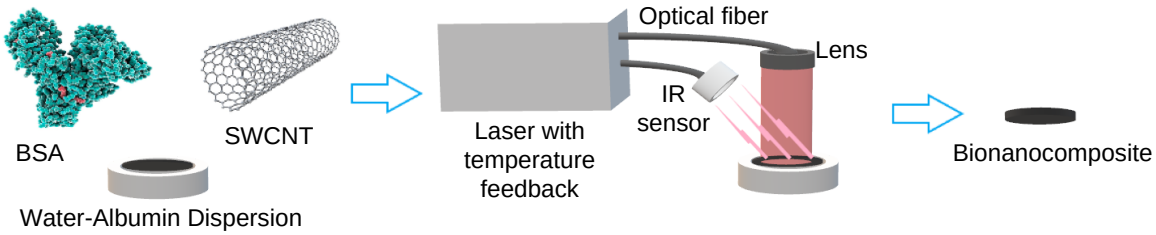

Figure 3. The creation scheme of the SWCNT-based composites in BSA matrix.

Absorption spectra of samples were recorded using Nicolet iS50 Thermo Scientific Fourier transform spectrometer. IR absorption spectra were measured in range 500–4000 cm^{-1} at room temperature. Bionanocomposite samples were crushed into fragments and KBr pellets were made from them. Thickness of the samples for IR spectroscopy was ~1 mm. IR absorption spectra were averaged over 256 scans for each sample, and the spectral resolution was 1 cm^{-1}. Raman spectra were obtained on a LabRAM HR Evolution HORIBA Scientific spectrometer. Spectra were excited by radiation from semiconductor laser with wavelength 633 nm, power up to 0.5 W (depending on the signal-to-noise ratio) and lasting 10 seconds. Spectra were measured at room temperature. Curves were averaged over 150 scans, recorded with resolution of 1 cm^{-1}, and subjected to inverse Fourier transform.

3. RESULTS AND DISCUSSION

3.1 Effect of defects on Raman spectrum of SWCNT graphene plane

Various types of defects were modeled by nature (vacancy defect inside graphene sheet, boundary defect due to absence of hydrogen atoms, vacancy defect, or bond breaking between carbon atoms at the edge of graphene plane.

In case of topological defect in form of vacancy defect in hexagonal structure inside graphene, the intensity of both D and D' bands increases in Raman spectrum, but intensity of D' line is stronger than intensity of D line (Figure 4). Decrease in hydrogen atoms at the boundary of graphene sheet leads to strong decrease in G and D' lines in Raman spectrum, where practically only one D line remains. It should be noted that in all the above cases, 2D line did not appear in 2700 cm^{-1} region.

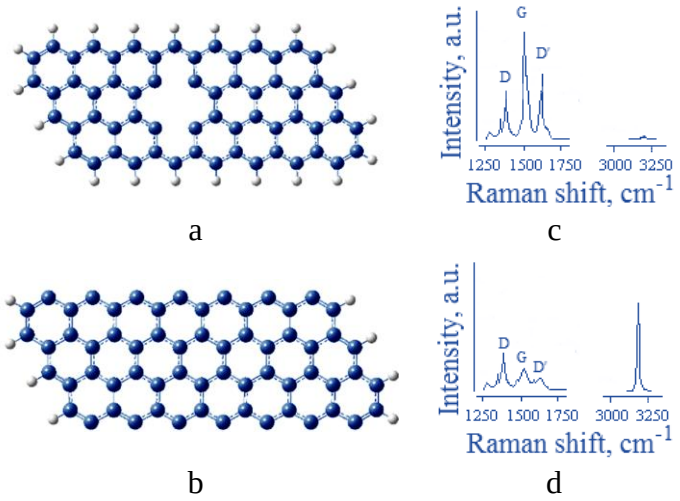

Figure 4. Molecular models of graphene sheet with vacancy defect inside the graphene sheet (a) and the boundary defect due to absence of hydrogen atoms (b). Their Raman spectra: defect inside the graphene sheet (c) and without hydrogen atoms at two borders (d).

In Figure 5 evolution of atomic structure in time and space with different numbers of surrounding hydrogen atoms is shown. Various options were obtained for formation of structure and formation of CH bonds (Figure 5c,d) depending on arbitrary environment (Figure 5b). The diversity of resulting structural fragments can be quite large due to the fact that hydrogen and carbon atoms can be located unevenly and in different numbers along the edges of graphene.

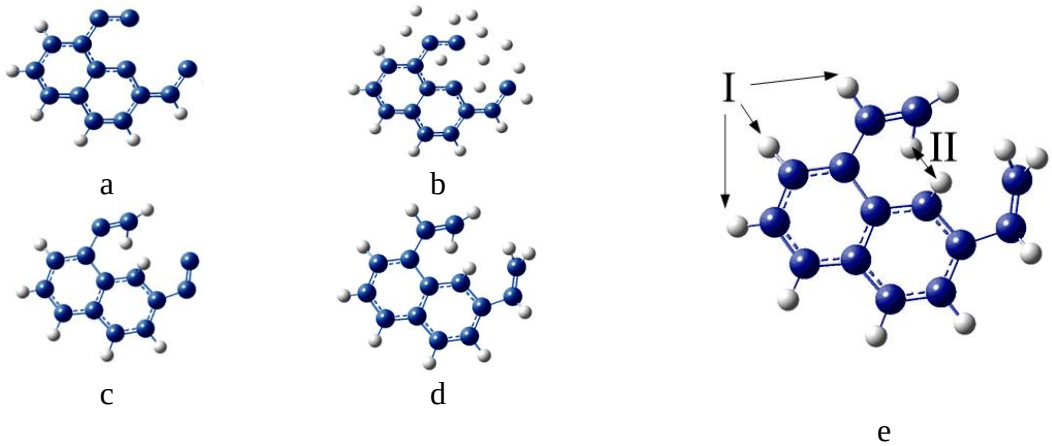

Figure 5. Initial area of the defect (a), example of its surrounding with hydrogen atoms (b), results of structure optimization (c, d), which were obtained for different positions of hydrogen atoms near the defect and region of the defect with hydrogen atoms in environment, explaining the vibrations (e).

Graphene fragment (Figure 6a) doped with nitrogen atoms (Figure 6b) and functionalized with oxygen atoms (Figure 6c) was modeled. As experimental Raman spectra, we used digitized data from works in which monolayer of graphene membrane[29], nitrogen-doped graphene[38], and reduced graphene oxide[39] was studied. Theoretical ones are calculated according to fragment models (Figure 5d-f).

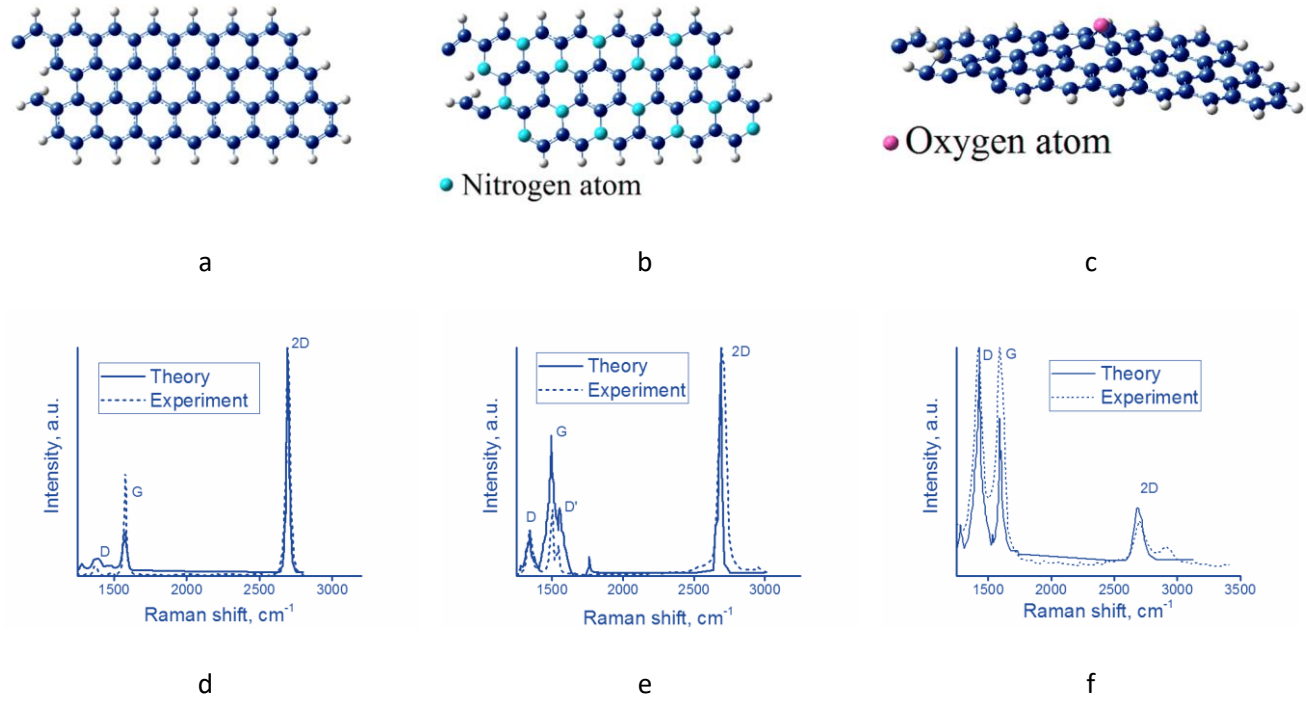

Figure 6. Molecular models of graphene sheets with a vacancy defect in the hexagonal structure, which is located on the edge: fragment with parallelogram shape (a); intercalated by nitrogen atoms (b) and functionalized by oxygen atoms (c). The following are the theoretical and experimental Raman spectra, respectively: fragment with parallelogram shape (d); intercalated by nitrogen atoms (e) and functionalized by oxygen atoms (f).

Common for all structures are steric obstacles that arise during vibrations of hydrogen atoms covalently bonded to neighboring carbon atoms (Figure 5e). In case I (Figure 5e), hydrogen atoms do not interfere with each other during vibrations. Close arrangement of hydrogen atoms interferes with their vibrations (Figure 5e, case II). In this regard, decrease in frequency of stretching vibration q(CH) is observed, which for all molecular fragments is manifested in the region of ~2700 cm^{-1}. Theoretical Raman spectra agree well with experimental dependences. Differences in spectra are due to presence of several defects of different nature in real graphene at once. In theoretical and experimental spectra, the strongest band D in graphene and functionalized by oxygen atoms graphene (Figure 6f) is observed, and in graphene doped with nitrogen atoms, the strongest band D' (Figure 6e). The strongest 2D band is characteristic of the model (Figure 6d), doping and functionalization of graphene sheet leads to decrease in its intensity.

Thus, in this work, we examined the effect of vacancy defects inside and on the edge of graphene sheet on the intensities of D, D', and 2D lines. Feature of topological defect in form of vacancies inside graphene sheet is excess of D' band intensity over D band intensity (Figure 4). Therefore, in case of intensities ratio of $I_{D'}/I_D>1$ bands, one can judge the presence of such defects. The 2D line, as was shown in this paper, is associated with presence of defect caused by absence of carbon atom at the edge of graphene sheet. Using it, it is possible to obtain qualitative and quantitative information on the process of graphene oxide reduction, treatment with ultraviolet radiation[40], or on the local number of graphene monolayers[41]. Analysis of D 'and 2D bands is necessary for dehydrogenation of graphene[42]. It is possible since the partial or complete absence of hydrogen atoms at the boundary of graphene sheet leads to disappearance of G and D'

lines in Raman spectrum (Figure 1d), and presence of nitrogen and oxygen atoms causes decrease in intensity of 2D line (Figure 5,6).

Ratio of G and 2D bands intensities (Figure 6d) in case of graphene experimental study can be different depending on number of monolayers, which is clearly shown by their distribution map[43]. After doping with nitrogen (Figure 6e), band D may exceed G[44]. This can be explained by different number of defects inside the sheet itself or by partial absence of hydrogen atoms at its edges (Figure 4). During the oxidation of graphene in Raman spectrum, not only contribution from functionalization by oxygen atoms (Figure 6f), but from other groups of atoms can be observed. Raman spectrum is also affected by different concentrations of functionalization and doping components[45]. Quantitative ratio of oxygen and carbon atoms increases the intensity ratio of band D to G[46].

3.2 Interaction of bovine serum albumin with single-wall carbon nanotubes in a bionanocomposite

It is known that amino acid residues of BSA - aspartic (Asp) and glutamic (Glu) are polar and have negative charge at physiological pH values. In radicals of acidic amino acids there is an additional carboxyl group. This group can form a chemical bond with side chains of other amino acids, while forming a tertiary proteins structure. Also, carboxyl group can chemically bind to external molecular structures. Figure 7 shows molecular structure of one of the BSA subdomains. Carboxyl groups of amino acid residues Glu and Asp were identified on the structure, most of which are located on the outer surface of protein molecule.

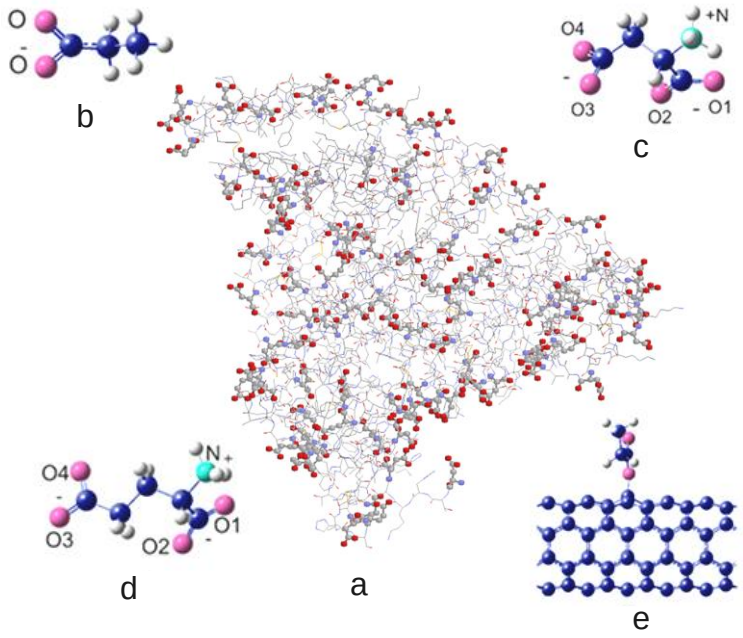

Figure 7. Structure of BSA subdomain with designation of carboxyl groups in Glu, Asp (a) and molecular fragment (b) entering into the side chain of Asp (c) and Glu (d) and forming a covalent bond with SWCNT (e).

To clarify the nature of interaction between BSA and SWCNTs, calculation was performed in which structural fragment of albumin, which has negative charge and is part of amino acid residues Asp and Glu, was chosen as molecular model (Figure 7). According to calculation results, this structural fragment of amino acid residues Asp and Glu (Figure 7b) forms a covalent bond with SWCNTs (nanotube diameter 1.7 nm). Energy of this bond was 580 kJ/mol, and its length was 1.42 Å.

Laser irradiation of BSA and SWCNT dispersion leads to initiation of chemical reaction between negatively charged amino acid residues Asp and Glu and nanotubes and, accordingly, formation of covalent bonds between them.

In spectrum of albumin, like other proteins, one can distinguish characteristic vibrations of polypeptides amide group. These are oscillations with frequency near 1650 cm^{-1} and 1540 cm^{-1}. Vibrational shape near 1650 cm^{-1} is mainly determined by change in length of C=O peptide bond. For oscillations with frequency near 1540 cm^{-1}, the peak shape is mixed and is determined by changes in CNH angle and CN bond length. These vibrations are commonly called vibrations of Amide I and Amide II, respectively. Analysis of frequencies and intensities of absorption bands and lines of Raman vibrations of amide group is widely used to establish the conformational structure of polypeptide chain.

Experimental measurement of FTIR and Raman spectra of BSA was performed and vibrational spectra of the zwitterionic forms of 20 amino acids and their dipeptides were calculated. It was found that vibrational forms of lateral residues of amino acids forming polypeptide do not mix with vibrational forms of amide fragment (Amide I, Amide II and Amide III). This allows them to be used to interpret vibrational FTIR and Raman spectra of BSA. Comparison of experimental and calculated BSA spectra showed that each experimental albumin absorption band is a superposition of several absorption bands of lateral amino acid residues. In this case, influence of intermolecular interactions between amino acid residues leads to shift in maximum and change in the intensity of absorption bands corresponding to vibrations of Amide I, Amide II, and Amide III. Overlapping of absorption bands of amino acid residues with absorption band of Amide I makes it very sensitive to structural changes. In particular, absorption band of Amide I is sensitive to manifestation of intermolecular interactions, as a result of which shift in frequency and intensity of this band makes it possible to determine structural changes in protein. Analysis of intensities of vibrational spectra of amino acid residues in the 1540 cm^{-1} region showed that intermolecular interactions lead to more significant change in intensity of absorption band of Amide II in the FTIR spectrum compared to Raman spectrum. In vibration region of Amide III (~1300-1200 cm^{-1}), deformation δ(OH) and δ(NH) vibrations of side chains of number of amino acids that participate in intermolecular interaction are manifested. As a result, values of corresponding frequencies of bending vibrations of Amide III can be shifted. In addition, a broad absorption band of medium intensity appears in experimental FTIR spectrum of BSA at 660 cm^{-1}. According to calculation, deformation vibrations of angles γ(COO), γ(COC), and γ(OCO-) of amino acid residues Glu and Asp are manifested in this spectral range. Participation of Glu and Asp in intermolecular interaction with other amino acid residues leads to shift in vibrational frequency of this deformational vibration and broadening of corresponding absorption band.

In Figure 7a-d experimental FTIR spectra of BSA and solid composites with different concentrations of SWCNT 1 – 0.01, c – 0.1, d – 1 g/L are shown.

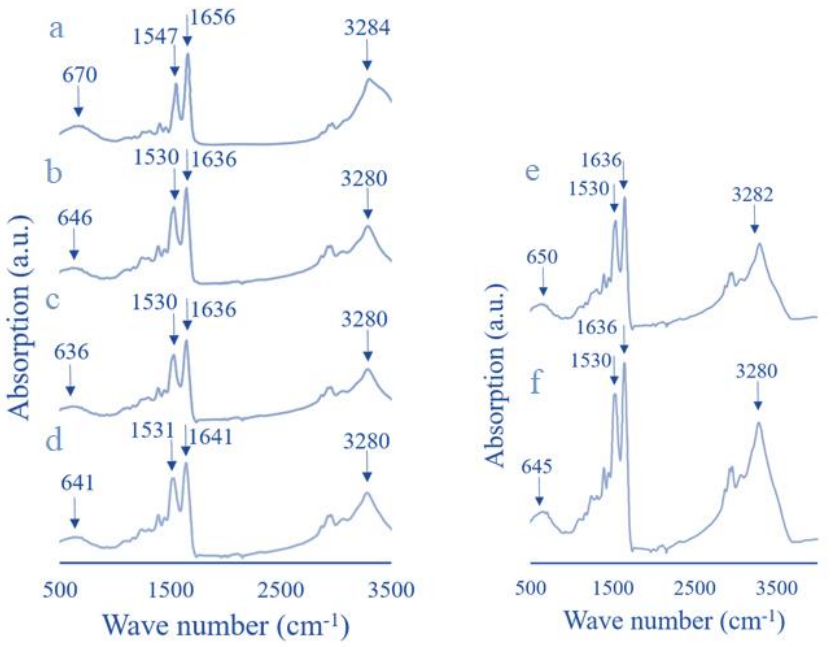

Figure 8. FTIR spectra of BSA (a) and BSA solid composites with SWCNT 1 with concentration of 0.01 (b), 0.1 (c), 1 (d) g/L and BSA composites with SWCNT 2 with concentration of 0.01 (e) and 0.1 (f) g/L.

Interaction between negatively charged amino acid group of COO amino acid residues Asp and Glu and carbon atoms of nanotubes (C_{SWCNT}) leads to formation of C_{SWCNT}–O covalent bonds and C_{SWCNT}O bond angles. This affects the values of vibration frequencies and intensities of absorption bands in the region of vibration of Amide I, Amide II, and 650 cm^{-1}. Such an effect is observed in spectra of solid composites with different SWCNT concentrations in Figure 8a-d. Comparison of FTIR spectra of composites at different concentrations of nanotubes shows that each spectrum is superposition of two spectra — with and without covalent bonds (Figure 8b-d). Obviously, an increase in concentration of nanotubes leads to saturation of SWCNT functionalization with oxygen atoms of amino acid residues Asp and Glu. In total spectrum at nanotube concentration of 1 g/mol, BSA spectrum prevails. Increase in diameter of tubes from 1.7 to 4 nm in composite does not lead to strong change in FTIR spectrum, as was the case with BSA spectrum and with spectra of composites with different nanotube concentrations. This is due to steric factor, which complicates interaction of albumin with nanotubes through the formation of covalent bonds. Changes in composites spectra with increase in concentration of nanotubes from 0.01 to 1 g/L have demonstrated single cases of covalent addition of albumin to larger nanotubes (Figure 8e-f).

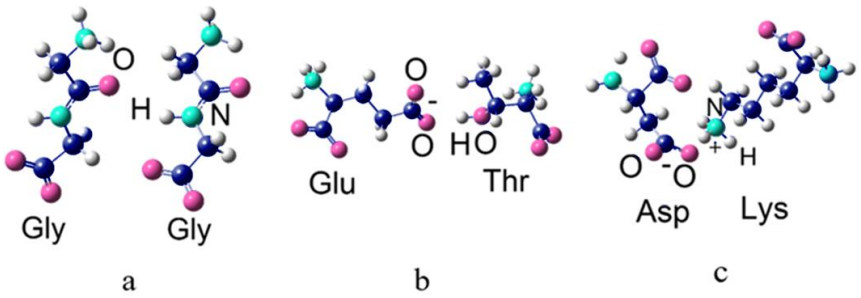

Figure 9. Molecular structures forming hydrogen Gly: Gly (a), ion-dipole Glu: Thr (b) and ion-ion Asp: Lys (c) intermolecular bonds in albumin.

To determine the effect of intermolecular interactions on vibrational spectra of proteins, we calculated the structure and vibrational spectra of albumin complexes: Gly: Gly, Glu: Thr, and Asp: Lys. This made it possible to take into account three types of intermolecular interactions – hydrogen, ion–dipole, and ion–ion bonds (Figure 9). Considered types of bonds can be used for qualitative assessment of intermolecular interactions between neutral and charged groups of side chain Rm–OH...COO(-)–Rn and between charged groups of side chains inside protein molecule Rm–NH_3+...COO(-)–Rn.

Table 1 - Energy of intermolecular interaction (E) and frequency (ν, cm-1) of bond stretching vibrations

Structure	**Bond**	***E*, kJ/mol**	**Oscillation frequency and intensity**		
			ν_1, cm^{-1} (km/mol; Å^4/AMU)	**ν_2, cm^{-1}, (km/mol; Å^4/AMU)**	**Ratio**
Gly:Gly	O…HN	8	3412 (361;36)	3462 (321;17)	q(NH) Gly
Glu:Thr	$(COO)^-$…(OH)	133	3420 (282;1287)	3831 (89;163)	q(OH) Thr
Asp-Lys	$(COO)^-$ …(N^+H_3)	315	3126(1964;59)	3428 (54;147)	q(N^+H_3) Lys

According to calculation, the energy of intermolecular interaction varies over a wide range – from 8 to 315 kJ/mol (Table 1). Magnitude of shift in vibrational frequency upon breaking of intermolecular bonds also varies over a wide range of 50 – 400 cm^{-1}, and intensity of the IR absorption and Raman bands can decrease by ~100 times. In Table 1, frequencies of stretching vibrations of NH and N+H before and after breaking the intermolecular bonds are denoted as ν1 and ν2, respectively. Values of intensities of IR bands (km/mol) and Raman (Å^4/AMU) are given in parentheses.

Strong decrease in composites absorption bands intensities for different concentrations of nanotubes (Figure 8a-d), as well as shift in frequencies of valence vibrations in high-frequency region, shows that conformational changes in secondary and tertiary structures of BSA. For SWCNT 2 (with large diameter of 4 nm), such characteristic changes are not observed.

Obviously, formation of covalent bonds should also appear in Raman spectra of composites. Note that for ideal (defect-free) nanotube, Raman spectrum exhibits radial-respiratory (low-frequency region ~200 cm^{-1}) and tangential (high-frequency region ~1600 cm^{-1}) vibrations. Tangential longitudinal and radial vibrations together form a G-band. In region of ~1300 cm^{-1}, there is a line characterizing presence of various defects caused by imperfection of nanotube lattice and presence of impurities. Other modes have very low intensity and are practically not observed in Raman spectrum.

In Figure 10 Raman spectra of pure BSA, SWCNT 1 and solid composite with SWCNT 1, concentration of which was 0.01 and 1 g/L are shown.

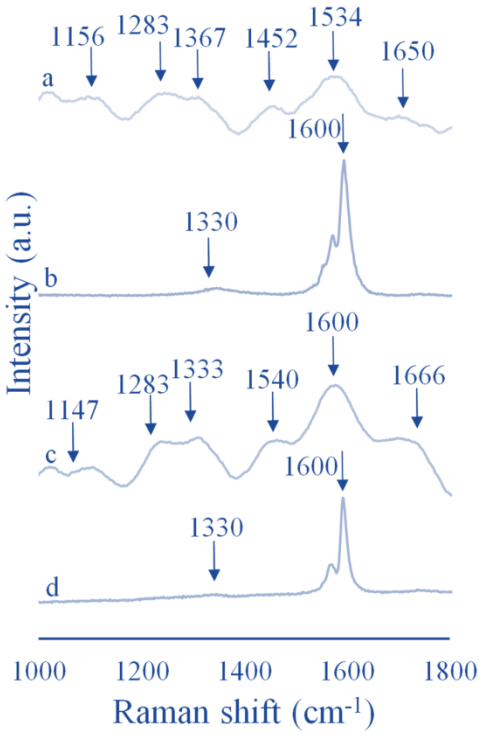

Figure 10. Raman spectra for BSA (a), SWCNT I (b) and BSA bionanocomposites with SWCNT I with a concentration of 0.01 (c) and 1 (d) g/l.

In Raman spectrum of SWCNTs, band intensity in ~1330 cm^{-1} region is significantly lower than band intensity of 1600 cm^{-1}, which indicates high purity and ideality of nanotubes structure. In Raman spectrum of composite with low concentration of nanotubes (0.01 g/L), significant increase in band intensity is observed in the region of ~1330 cm^{-1}. Band intensity in ~1330 cm^{-1} region becomes comparable with band intensity in ~1600 cm^{-1} region (Figure 10c). This confirms presence of significant number of defects in SWCNT composite. Defects are caused by covalent attachment of oxygen to graphene surface of nanotubes. Raman spectra of composites at different concentrations of nanotubes are superposition of two spectra – with and without covalent bonds. Increase in concentration of nanotubes leads to saturation of SWCNTs functionalization with oxygen atoms of amino acid residues Asp and Glu. This is confirmed by the fact that Raman spectrum of SWCNTs prevails in total spectrum of composite at high nanotube concentration of 1 g/L.

4. CONCLUSIONS

A method for formation of bionanocomposites that can be used as coatings for implantable devices interacting with blood is proposed. For example, they can be used to control the state of blood cells aggregation. Such composites are composed of albumin blood protein and SWCNTs. They are formed by evaporation of water-albumin dispersion of nanotubes by diode laser with precise temperature control. Influence of various types of SWCNT graphene plane defects on formation of frame structure from them and albumin was determined using Raman and FTIR spectroscopy methods.

It was found that shape of graphene sheet affects intensity of D and D' bands in its Raman spectrum. The strongest increase in intensity of D band compared to G band is observed in case of partial or complete absence of hydrogen atoms at the boundary of graphene sheet, which leads to practical disappearance of G and D' lines in Raman spectrum. Molecular modeling showed that for structural defects there is steric hindrance to the edge of graphene sheet, which

occurs when vibrations of neighboring hydrogen atoms are moving towards each other. This leads to decrease in frequency of stretching vibration q(CH), which manifests itself in region of ~2700 cm^{-1} and corresponds to 2D vibration. Nature of 2D line origin was confirmed by comparing calculated and experimental Raman spectra with allowance for edge defects.

Molecular modeling method showed the possibility of functionalization of nanotubes by oxygen atoms of negative amino acid residues Asp and Glu located on the outer surface of BSA. Formation of covalent bonds between BSA and SWCNT is confirmed by FTIR and Raman spectra. Spectra were recorded for small diameter nanotubes (1.7 nm) with various concentrations (0.01, 0.1, and 1 g/mol). Comparison of FTIR spectra of composites for different concentrations of nanotubes shows that each spectrum is a superposition of two spectra – with and without covalent bonds. An increase in nanotubes concentration leads to saturation of SWCNT functionalization with oxygen atoms of amino acid residues Asp and Glu.

Covalent interaction of BSA with SWCNTs disrupts the secondary and tertiary structures of albumin. This is confirmed by significant decrease in intensity of absorption bands in high-frequency region. Vibrational spectra of three complexes Gly: Gly, Glu: Thr, and Asp: Lys were calculated, which allows to take into account hydrogen, ion-dipole, and ion-ion bonds in case of intermolecular interaction between amino acid residues. This made it possible to detect a significant decrease in intensity of absorption bands in the region of stretching vibrations of OH and NH bonds. Formation of covalent bond between BSA and SWCNTs in bionanocomposite leads to increase in band intensity in ~1330 cm^{-1} region on Raman spectrum compared with the spectrum of initial nanotubes. This confirms presence of significant defects in SWCNTs caused by covalent addition of oxygen to graphene surface of nanotubes. It was found that increase in nanotubes diameter (4 nm) and their concentration in composite practically does not affect vibrational spectra, which confirms hydrophobic interaction of BSA and SWCNTs.

Thus, two types of interactions in solid bionanocomposites based on BSA with SWCNTs – hydrophobic and with formation of covalent bonds – depend on the diameter of nanotubes used. This criterion makes it possible to widely use frame composite materials in biomedicine, depending on requirements for quality of their manufacturing and use.

ACKNOWLEDGEMENTS

This study was supported by the Russian Science Foundation (Project No. 20-49-04404), Russian academic excellence project "5-100" for Sechenov First Moscow State Medical University. The studies were performed using MIET Core facilities center "MEMS and electronic components.

REFERENCES

[1] Zhao, P., Gu, H., Mi, H., Rao, C., Fu, J., Turng, L., “Fabrication of scaffolds in tissue engineering: A review,” Frontiers of Mechanical Engineering 13(1), 107-119 (2018).

[2] Ashtari, K., Nazari, H., Ko, H., Tebon, P., Akhshik, M., Akbari, M., Alhosseini, S. N., Mozafari, M., Mehravi, B., Soleimani, M., Ardehali, R., Warkiani, M. E., Ahadian, S., Khademhosseini, A., "Electrically conductive nanomaterials for cardiac tissue engineering," Advanced Drug Delivery Reviews 144, 162-179 (2019)

[3] Chandarana, M., Curtis, A. and Hoskins, C., "The use of nanotechnology in cardiovascular disease," Applied Nanoscience 8(7), 1607-1619 (2018).

[4] Maduraiveeran, G., Sasidharan, M., Ganesan V., “Electrochemical sensor and biosensor platforms based on advanced nanomaterials for biological and biomedical applications,” Biosensors and Bioelectronics 103, 113-129 (2018).

[5] Hu, X. L., Kwon, N., Yan, K. C., Sedgwick, A. C., Chen, G. R., He, X. P., James, T. D., Yoon, J., “Bio-Conjugated Advanced Materials for Targeted Disease Theranostics,” Advanced Functional Materials, 1907906 (2020).

[6] Kim, H., Beack, S., Han, S., Shin, M., Lee, T., Park, Y., Kim, K. S., Yetisen, A. K., Yun, S. H., Kwon, W. and Hahn, S. K., "Multifunctional photonic nanomaterials for diagnostic, therapeutic, and theranostic applications," Advanced Materials 30(10), 1701460 (2018).

[7] Zhang, A. and Lieber, C. M., "Nano-bioelectronics," Chemical reviews 116(1), 215-257 (2016).

[8] Sauvage, F., Schymkowitz, J., Rousseau, F., Schmidt, B. Z., Remaut, K., Braeckmans, K., and De Smedt, S. C., "Nanomaterials to avoid and destroy protein aggregates," Nano Today, 100837 (2020).
[9] Arunkumar R., Suaganya T., Robinson S., "Design and analysis of 2D photonic crystal based biosensor to detect different blood components," Photonic Sensors 9(1), 69-77 (2019).
[10] Carson, L., Hibbert, K., Akindoju, F., Johnson, C., Stewart, M., Kelly-Brown, C., Beharie, G., Fisher, T., Stone, J., Stoddart, D., Oki, A., Neelgund, G. M., Regisford, G., Traisawatwong, P., Zhou, J., Luo, Z., "Synthesis, characterization and stability of chitosan and poly(methylmethacrylate) grafted carbon nanotubes," Spectrochimica Acta Part A Molecular and Biomolecular Spectroscopy 96, 380-386 (2012).
[11] Zanello, L. P., Zhao, B., Hu, H., Haddon, R. C., "Bone cell proliferation on carbon nanotubes," Nano Letters 6(3), 562–567 (2006).
[12] Hirata, E., Uo, M., Nodasaka, Y., Takita, H., Ushijima, N., Akasaka, T., Watari, F., Yokoyama, A., "3D collagen scaffolds coated with multiwalled carbon nanotubes: initial cell attachment to internal surface," Journal of Biomedical Matererials Research Part B Applied Biomaterials 93B(2), 544–550 (2010) .
[13] Gerasimenko, A. Yu., Ichkitidze, L. P., Podgaetsky, V. M., Selishchev, S. V., "Biomedical applications of promising nanomaterials with carbon nanotubes," Biomedical Engineering 48(6), 310–314 (2015).
[14] Gerasimenko, A. Yu., Kitsyuk, E. P., Kuksin, A. V., Ryazanov, R. M., Savitskiy, A. I., Saveliev, M. S., Pavlov, A. A., "Influence of laser structuring and barium nitrate treatment on morphology and electrophysical characteristics of vertically aligned carbon nanotube arrays," Diamond and Related Materials 96, 104-111 (2019).
[15] Dovbeshko, G. I., Fesenko, O. M., Obraztsova, E. D., Allakhverdiev, K. R., Kaja, A. E., "Conformation analysis of nucleic acids and proteins adsorbed on single-shell carbon nanotubes," Journal of Structural Chemistry 50(5), 954-961 (2009).
[16] Holt, B. D., Dahl, K. N., Islam, M. F., "Quantification of Uptake and Localization of Bovine Serum Albumin-Stabilized Single-Wall Carbon Nanotubes in Different Human Cell Types," Small 7(16), 2348 (2011).
[17] Li, L., Lin, R., He, H., Jiang, L., Gao, M., "Interaction of carboxylated single-walled carbon nanotubes with bovine serum albumin," Spectrochimica Acta Part A: Molecular and Biomolecular Spectroscopy 105, 45-51 (2013).
[18] Lu, F., Gu, L., Meziani, M. J., Wang, X., Luo, P. G., Veca, L. M., Cao, L., Sun, Y.-P., "Advances in Bioapplications of Carbon Nanotubes," Advanced Materials 21(2), 139–152 (2009).
[19] Thamwattana, N., Baowan, D., Cox, B. J., "Modelling bovine serum albumin inside carbon nanotubes," RSC Advances 3(45), 23482-23488 (2013).
[20] Muzi, L., Tardani, F., La Mesa. C,, Bonincontro, A., Bianco, A., Risuleo, G., "Interactions and effects of BSA-functionalized single-walled carbon nanotubes on different cell lines," Nanotechnology 27(15), 155704 (2016).
[21] Ichkitidze, L. P., Gerasimenko, A. Yu., Podgaetsky, V. M., Selishchev, S. V., "Layers with the tensoresistive properties and their possible applications in medicine," Materials Physics and Mechanics 37(2), 153-158 (2018).
[22] Privalova, P. Yu., Gerasimenko, A. Yu., Zhurbina, N. N., Petukhov, V. A., Pyankov, E. S., Ichkitidze, L. P., Suetina, I. A., Mezentseva, M. V., Russu, L. I., "Electrical Stimulation of Human Connective Tissue Cells on Layers of Composite Structures with a Nanocarbon Framework," Biomedical Engineering 52(5), 8-10 (2018).
[23] Savelyev, M. S., Vasilevsky, P. N., Gerasimenko, A. Yu., Ichkitidze, L. P., Podgaetsky, V. M., Selishchev, S. V., "Nonlinear optical characteristics of albumin and collagen dispersions with single-walled carbon nanotubes," Materials Physics and Mechanics 37, 133-139 (2018).
[24] Zhurbina, N. N., Kurilova, U. E., Ichkitidze, L. P., Podgaetsky, V. M., Selishchev, S. V., Suetina, I. A., Mezentseva, M. V., Eganova, E. M., Pavlov, A. A., Gerasimenko, A. Yu., "Investigation of cell proliferative activity on the surface of the nanocomposite material produced by laser radiation," Proceedings of SPIE 9917, 991718-1 – 991718-7 (2016)

[25] Gerasimenko, A. Yu., Ichkitidze, L. P., Podgaetsky, V. M., Savelyev, M. S., Selishchev, S. V., "Laser nanostructuring 3-D bioconstruction based on carbon nanotubes in a water matrix of albumin," Proceedings of SPIE 9887, 988725-1 – 988725-10 (2016).
[26] Gerasimenko, A. Yu., Zhurbina, N. N., Kurilova, U. E., Ichkitidze, L. P., Selishchev, S. V., Suetina I. A., Mezentseva, M. A., Russu, L. I., Zar, V. V., Podgaetskii, V. M., "Knee Joint Ligament Implants with Composite Nanocoatings," Biomedical Engineering 20(3), 206-209 (2016).
[27] Childres, I., Jauregui, L. A., Park, W., Cao, H., Chen, Y. P., "Raman Spectroscopy of Graphene and Related Materials," in: J. I. Jang (Ed.), New Dev. Phot. Mater. Res., Nova publ., New York, United States, 424 (2013).
[28] Zhao, T., Liu, Z., Xin, X., Cheng, H.-M., Ren, W., "Defective graphene as a high-efficiency Raman enhancement substrate," Journal of Materials Science 35, 1996–2002 (2019).
[29] Hu, K.-M., Xue, Z.-Y., Liu, Y.-Q., Song, P.-H., Le, X.-H., Peng, B., Yan, H., Di, Z.-F., Xie, J., Lin, L.-W., Zhang, W.-M., "Probing built-in stress effect on the defect density of stretched monolayer graphene membranes," Carbon N. Y. 152, 233–240 (2019).
[30] Pawbake, A. S., Mishra, K. K., Machuno, L. G. B., Gelamo, R. V., Ravindran, T. R., Rout, C. S., Late, D. J., "Temperature and pressure dependent Raman spectroscopy of plasma treated multilayer graphene nanosheets," Diamond and Related Materials 84, 146–156 (2018).
[31] Savelyev, M. S., Gerasimenko, A. Y., Podgaetskii, V. M., Tereshchenko, S. A., Selishchev, S. V., Tolbin, A. Y., "Conjugates of thermally stable phthalocyanine J-type dimers with single-walled carbon nanotubes for enhanced optical limiting applications," Optics and Laser Technology117, 272–279 (2019).
[32] Heller, E. J., Yang, Y., Kocia, L., Chen, W., Fang, S., Borunda, M., Kaxiras, E., "Theory of Graphene Raman Scattering," ACS Nano 10, 2803–2818 (2016).
[33] Eckmann, A., Felten, A., Mishchenko, A., Britnell, L., Krupke, R., Novoselov, K.S., Casiraghi, C., "Probing the Nature of Defects in Graphene by Raman Spectroscopy," Nano Letters 12, 3925–3930 (2012).
[34] Gerasimenko, A. Y., Ichkitidze, L. P., Piyankov, E. S., Pyanov, I. V., Rimshan, I. B., Ryabkin, D. I., Savelyev, M. S., Podgaetskii, V. M., "Use of indocyanine green in nanocomposite solders to increase strength and homogeneity in laser welding of tendons," Biomedical Engineering 50(5), 310–313 (2017).
[35] Rimshan, I. B., Zhurbina, N. N., Kurilova, U. E., Ryabkin, D. I., Gerasimenko, A. Y., "Biocompatible nanomaterial for restoration of continuity of dissected biological tissues," Biomedical Engineering 52(1), 23–26 (2018).
[36] Gerasimenko, A. Yu., Gubarkov, O. V., Ichkitidze, L. P., Podgaetskii, V. M., Selishchev, S. V., Ponomareva, O. V., "Nanocomposite solder for laser welding of biological tissues," Semiconductors 45(13), 93-98 (2011).
[37] Gerasimenko, A. Yu., Ten, G. N., Ryabkin, D. I., Shcherbakova, N. E., Morozova, E. A., Ichkitidze, L. P., "The study of the interaction mechanism between bovine serum albumin and single-walled carbon nanotubes depending on their diameter and concentration in solid nanocomposites by vibrational spectroscopy," Spectrochimica Acta Part A: Molecular and Biomolecular Spectroscopy 227(117682), 1-10 (2020).
[38] Gao, H., Song, L., Guo, W., Huang, L., Yang, D., Wang, F., Zuo, Y., Fan, X., Liu, Z., Gao, W., Vajtai, R., Hackenberg, K., Ajayan, P. M., "A simple method to synthesize continuous large area nitrogen-doped graphene," Carbon N. Y. 50, 4476–4482 (2012).
[39] Díez-Betriu, X., Álvarez-García, S., Botas, C., Álvarez, P., Sánchez-Marcos, J., Prieto, C., Menéndez, R., De Andrés, A., "Raman spectroscopy for the study of reduction mechanisms and optimization of conductivity in graphene oxide thin films," Journal of Materials Chemistry C 1, 6905 (2013).
[40] Iqbal, M. Z., Siddique, S., Rehman, A., "Structural defects controlled oxidation of UV irradiated graphene-based field effect transistors," Diamond and Related Materials 85, 112–116 (2018).
[41] Ferrari, A. C., Meyer, J. C., Scardaci, V., Casiraghi, C., Lazzeri, M., Mauri, F., Piscanec, S., Jiang, D., Novoselov, K. S., Roth, S., Geim, A. K., "Raman Spectrum of Graphene and Graphene Layers," Physical Review Letters 97(18), 187401 (2006).

[42] Luo, Z., Yu, T., Ni, Z., Lim, S., Hu, H., Shang, J., Liu, L., Shen, Z., Lin, J., "Electronic Structures and Structural Evolution of Hydrogenated Graphene Probed by Raman Spectroscopy," The Journal of Chemical Physics 115, 1422–1427 (2011).
[43] Lebedev, A. A., Lebedev, S. P., Novikov, S. N., Davydov, V. Y., Smirnov, A. N., Litvin, D. P., Makarov, Y. N., Levitskii, V. S., "Supersensitive graphene-based gas sensor," Technical Physics 61, 453–457 (2016).
[44] Beams, R., Gustavo Cançado, L., Novotny, L., "Raman characterization of defects and dopants in graphene," Journal of Physics: Condensed Matter 27, 083002 (2015).
[45] Zhang, S., Li, Y., Kang, Y., Dong, Y., Hong, S., Chen, X., Zhou, J., Fedoseeva, Y. V., Asanov, I. P., Bulusheva, L. G., Song, H., Okotrub, A. V., "Leaky graphene oxide with high quantum yield and dual-wavelength photoluminescence," Carbon 108, 461–470 (2016).
[46] Babaev, A. A., Zobov, M. E., Kornilov, D. Y., Tkachev, S. V., Terukov, E. I., Levitskii, V. S., "Optical and Electrical Properties of Graphene Oxide," Optics and Spectroscopy 125, 1014–1018 (2018).